Functional Composites and Structures

Design and fabrication of bioinspired pattern driven magnetic actuators

To cite this article: Anasheh Khecho and Erina Baynojir Joyee 2024 *Funct. Compos. Struct.* **6** 015010

IOP Publishing Funct. Compos. Struct. 6 (2024) 015010 https://doi.org/10.1088/2631-6331/ad335f

Functional Composites and Structures

OPEN ACCESS

RECEIVED
14 December 2023

REVISED
22 February 2024

ACCEPTED FOR PUBLICATION
10 March 2024

PUBLISHED
22 March 2024

PAPER

Design and fabrication of bioinspired pattern driven magnetic actuators

Anasheh Khecho and Erina Baynojir Joyee*

Mechanical Engineering and Engineering Science, University of North Carolina at Charlotte, Charlotte, NC, United States of America
* Author to whom any correspondence should be addressed.

E-mail: ejoyee@charlotte.edu

Keywords: 3D printing, magnetic actuator, bioinspired additive manufacturing, rhombus structure, particle-polymer composite, magnetic particles, pattern-driven actuators

Supplementary material for this article is available online

Abstract

Additive manufacturing (AM) has drawn significant attention in the fabrication of soft actuators due to its unique capability of printing geometrically complex parts. This research presents the design and development of an AM process for bioinspired, deformable, and magnetic stimuli-responsive actuator arms. The actuator arms were fabricated via the material extrusion-based AM process with magnetic particle-polymer composite filaments. Inspired by the rhombus cellular structure found in nature, different design parameters, such as the line width of the interior rhombus sides, and 3D printing parameters were studied and optimized to fabricate actuator arms that exhibit enhanced flexibility while being magnetically actuated. The trigger distance and deformation experiments revealed that the width of the rhomboids' sides played a critical role in magnetic and bending properties. It was found that the sample with a line width of 550 μm and printing layer thickness of 0.05 mm had the maximum deflection with a measured bending angle of 34 degrees. The magnetic property measurement exhibited that the sample with a line width of 550 μm showed the maximum magnetic flux density of 3.2 mT. The trigger distance results also supported this result. A maximum trigger distance of 8.25 mm was measured for the arm with a line width of 550 μm. Additionally, tensile tests showed that the sample exhibited a 17.7 MPa tensile strength, 1.8 GPa elastic modulus, and 1.3% elongation. Based on these results, we successfully fabricated a 3D printed magnetic gripper with two rhombus cellular structured arms which showed grasping and extensive load lifting capability (up to ~140 times its weight).

1. Introduction

In recent years, there has been a growing interest in incorporating bioinspired structures in designing many mechanical systems, particularly in the soft actuators field. Soft actuators that are fabricated based on bioinspired structures such as hydrogel-based aquatic organisms, inchworm-inspired, leaf-like structures, and flexible actuators, exhibit significantly enhanced functionality compared to the non-nature-inspired design structures [1–3]. This is because bioinspired soft actuators offer a higher degree of compatibility for human-machine interaction due to their flexibility in design. Among different soft actuator systems, bioinspired actuators have specifically drawn major attention due to their shape-changing capability in response to external stimuli. These highly adaptive actuators can be designed into structures that are capable of complex shape changes leading to an enhanced actuating performance. In other words, stimuli-responsive smart actuators are highly desirable since they can generate mechanical deformation swiftly in a sophisticated manner, under different types of external stimuli. Researchers have demonstrated stimulus response materials based on various actuation principles including light [4, 5], electrical [6–8], heat [9, 10], photothermal [11], magnetic [12–14], pneumatic [15, 16], and chemical [17, 18] stimuli. Among these actuation methods, magnetic actuation garnered much attention since the magnetic field can penetrate most biological materials safely, and provide a fast and effective untethered actuation method [19, 20]. Magnetic

actuation is proven to be safe for humans and has already been heavily used in applications including magnetic resonance imaging, magnetic hyperthermia, and other biomedical applications such as soft grippers in minimally invasive surgery. This is because of the recent advancements in materials and fabrication techniques that have led to the development of numerous soft and rigid smart actuators exhibiting high performance on remote actuation and shape transformation across different designed structures [21–25]. These high-performance smart actuators are commonly made from magnetic particle-polymer composites in which the magnetic particles are dispersed uniformly in the polymer matrix [26]. These composites are widely used in magnetic actuators due to their capability of remote contactless actuation, rapid response, simple controlling of the systems, and specifically reversible deformability. Flexible magnetic composites that utilize iron particles with low remanence and low coercivity can achieve a high response of the structural deformation to the magnetic field [27]. Under an external magnetic field, a macroscopic deformation occurs and after removal of the external magnetic field, the reconfigurable magnetic composite materials can recover to the original position due to their inherent reversible properties.

On the other side, the fabrication of particle-polymer composite based bioinspired complex structures has become more feasible than ever with the development of additive manufacturing techniques such as digital light processing (DLP) [28–30], direct ink writing (DIW) [31–33], and fused deposition modeling (FDM) [34–36]. This technology has been widely adopted as a potential fabrication method for novel materials and composites (i.e., magnetic particle-polymer composites). For instance, Ji *et al* [37] employed the DLP method to print a magnetic driving gripper by creating magnetic and non-magnetic segments of Fe_3O_4 nanoparticles. The fabrication of photocurable resin-Fe_3O_4 composite via DLP was also studied to 3D print parts in which the movements of the part were readily controllable by an external magnetic field [38]. Inspired from nature, Joyee and Pan [39] used a magnetic field assisted DLP based 3D printing method to print a inchworm inspired soft robots. The actuation and locomotion of the multimaterial soft robot was controlled by magnetic field. Besides the photopolymerization techniques, various researchers have used extrusion-based methods to manufacture polymeric composites. The combination of PLA polymer and Fe_3O_4 particles through FDM method was investigated to build parts with shape memory ability and magnetic actuation [40]. In addition, Kim *et al* [41] used DIW to print a soft continuum robot manipulated by the magnetic field actuation of the NdFeB microparticles. Zhang *et al* [42] introduced 4D printing of magnetic NdFeB composites where the magnetization and traditional DIW were combined. In another study, Ma *et al* [43] combined the UV photopolymerization in DLP and the DIW method for the fabrication of parts having multimodal shape transformations with magnetic actuation.

Each of the mentioned techniques has its advantages and limitations. For example, while the DLP method offers high printing accuracy, it requires the use of photocurable polymers. On the other hand, DIW provides a wide range of material selections but retaining the material's shape after printing is challenging. Therefore, among different technologies, the simple working mechanism, low cost, and wide adaptability of the material in FDM have made this method the potential shaping process for magnetic actuators [44]. By utilizing FDM 3D printing methods, magnetic actuators can be structured with homogeneously dispersed magnetic particles [31, 32], or anisotropic magnetization profiles [30, 33, 42, 43]. Magnetization profiles can be achieved by patterning magnetic particles within the polymer matrix. However, despite the advantages of bioinspired magnetic actuators, proper magnetic actuation is possible when the homogeneous magnetic material is shaped accurately according to a dimensionally optimized bioinspired design. Additionally, although magnetic particle-polymer composites make a good candidate for untethered actuators, due to its brittle nature it is very hard to fabricate flexible actuator arm with high magnetization.

Bioinspired structures observed in nature are generally highly porous materials usually generated from the tessellation of simple geometrical patterns such as hexagonal, square, rhombus etc, exhibiting unique properties that facilitate high-strength–low-weight structures. Given their low weight, lattice structures are commonly observed in birds, in many marine organisms (e.g. bone, shell), and plants [45–47]. One of the fundamental patterns observed in nature is the pattern on *Sapium sebiferum* leaves (figure 1) [48]. Inspired by the pattern of the delicate leaves in nature and combining tessellation, the characteristics of current soft actuators can be promoted to a new level in which the lightweight, high aspect ratio actuators with high solid loading particles exhibit enhanced flexibility and bending strength in long actuation cycles with strong magnetization property. These structures are mostly surrounded by dense walls, forming sandwich structures. There is often a synergy between the cellular interior and the dense walls, resulting in varied mechanical characteristics. 3D printing provides easy control over manufacturing geometrically complicated designs. To our knowledge, most of the previously 3D printed magnetic actuators were in fact 2D and 2.5D structures and only a few of them were soft magnetic actuators with complex structures. In addition, although the *Sapium sebiferum* pattern is relatively uncomplicated, only a few researchers have studied this pattern as a potential infill pattern for soft actuators and particularly soft grippers. For soft gripping applications, the gripper arms should have a high elastic modulus (100 kPa–200 MPa) for a reversible

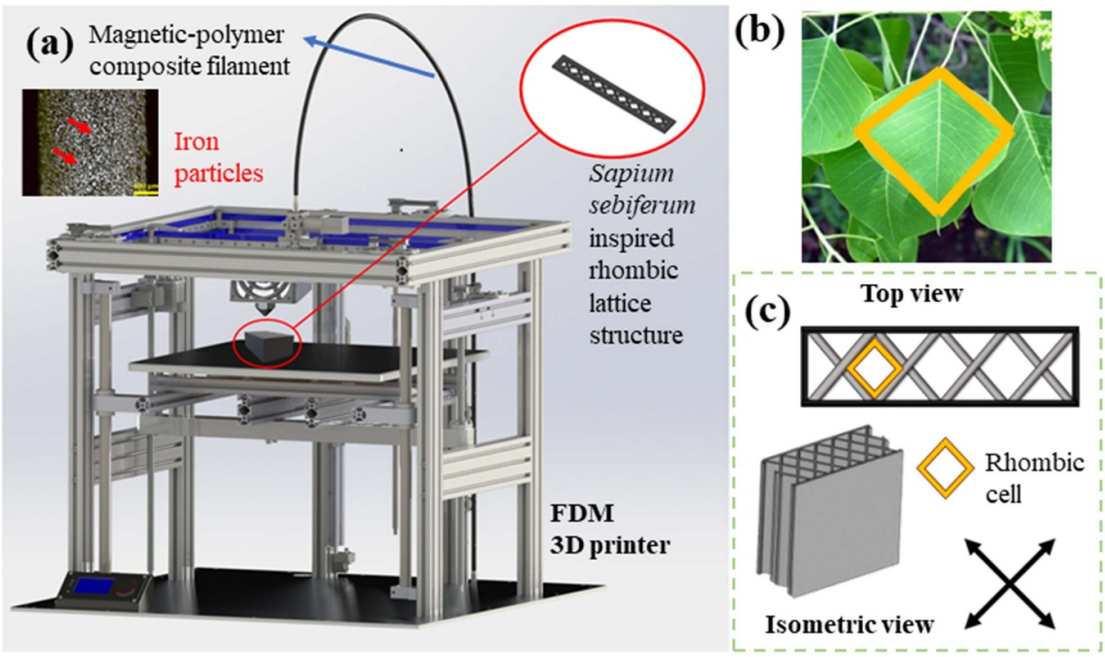

Figure 1. (a) The schematic of the 3D printing process for manufacturing bioinspired actuator arms; (b) *sapium sebiferum* leaves; (c) proposed bioinspired rhombic lattice sandwich pattern of the actuator arms.

deformation to grip the object [24]. From reviewing the literature, it can be concluded that, knowledge gaps exist in terms of finding relationship between geometrical and printing parameters with actuation efficiency (deformation capability and magnetic manipulation) in developing light weight untethered actuators.

Inspired by the promising features of bioinspired 3D printed structures and the need to address limitations in this area, this work focuses on the design and development of 3D printed stimuli-responsive magnetic actuator arms. Mimicking the natural rhombus cellular structure found in *Sapium sebiferum* (figure 1), we aim to fabricate highly flexible actuator arms with high strength and toughness that can tolerate long actuation cycles. These actuator arms have the potential to serve as effective grippers in various applications. The stiffness of the material which leads to different deformation profiles of the printed arms can be manipulated during the fabrication by changing the geometric parameters and printing the structure in patterns in computer-aided design (CAD) drawing.

2. Materials and methods

2.1. Materials

The bioinspired actuator arms were printed using thermoplastic particle-polymer composite filaments (Protoplant, Inc, Vancouver, WA) consisting of 45 wt % of ferromagnetic iron particles (finer than ∼44 μm) dispersed in a polylactic acid (PLA) matrix. The induction at magnetic saturation of the composite filament was 0.15 Tesla with relative (to air) permeability between 5 and 8. This magnetic PLA filament was brittle and abrasive compared to homogeneous PLA. Wear-resistant nozzles with inner diameters of 0.4 and 0.6 mm were tested and adjusted to find the optimal one.

2.2. Design and manufacturing of a bioinspired smart magnetic particle-polymer composite actuator arm

2.2.1. Design inspiration

In nature, lattice or cellular structures are very common, consisting of dense boundaries with a porous core. From bird feathers to mammalian bones, plants, etc, all have lattice porous structures to achieve high strength and low weight anatomy. Such structures are also known as *sandwich structures* (rhombic lattice structures encapsulated by solid exterior wall, figure 2(a)), which can provide resistance to local buckling that can result in failure in structure. Such bioinspired sandwich structures with dense exterior and lattice interior significantly increases the bending moment. For example, it has been shown experimentally that the critical buckling strength of the cylindrical-shaped sandwich porcupine quills is increased almost three times over hollow porcupine quills [49]. Among different cellular structures, the rhombus/diamond structure inspired from *Sapium sebiferum* leaves has advantages in buckling resistance and makes it easy to have locally tunable mechanical properties by changing geometrical parameters. Although PLA filament has good

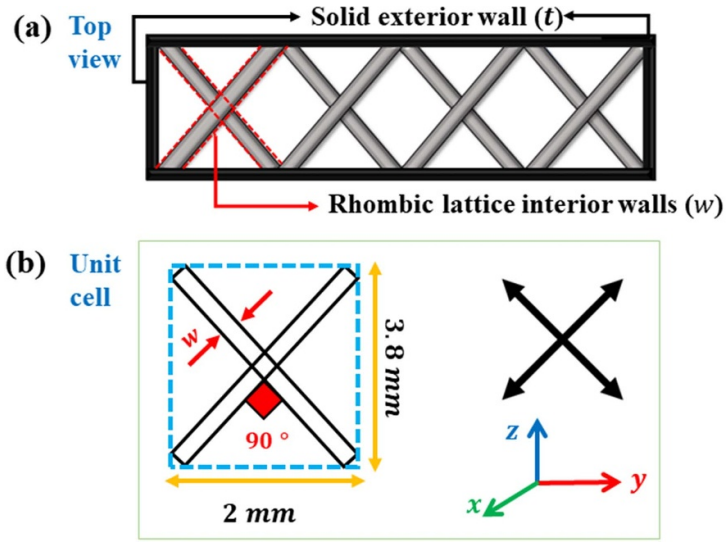

Figure 2. Different geometrical parameters of the proposed bioinspired rhombic lattice structures; (a) single actuator arm; (b) unit cell.

thermoplasticity and flexibility, mixing iron particles within the PLA makes it brittle. To achieve the desired flexibility and deformation needed in an actuator, a high-strength low weight bioinspired lattice rhombic sandwich structure was adopted in this study, taking inspiration from the above-mentioned biological organisms.

As shown in figure 2(a), the sandwich structures are composites of two phases: the dense exterior wall and the rhombic lattice interior cells (with different wall thicknesses w). As a result, the mechanical properties in terms of flexibility can be altered by changing the design parameters. The actuator arm design is geometrically parameterized by varied interior wall thickness w and the opening angle θ, set as 90 degrees. Other dimensions are shown in figure 2(b).

2.2.2. 3D design

The actuator arm has a smart magnetic particle-polymer composite structure with magnetic particles embedded in the body. The schematic of the digital model is shown in figure 3. The rhombus lattice design allows the actuator to be highly deformable. To support the structure, the rhombus pattern is surrounded by a dense wall and the inner area has rhombic lattice structures to increase flexibility without failure. The design parameters (figure 2) including the width of the rhomboid sides (w) and exterior wall thickness (t) were optimized to allow a synchronized movement with an activated magnetic field. The CAD model of the actuator was created in solidworks (version 2022, Concord, MA, UA) and then was sliced in Ultimaker Cura. The total length of each arm of the actuator is 30 mm (The 3D model of the actuator arm was designed based on a 30 × 5 × 0.5 mm rectangle sketch). Additionally, a fully solid sample having the same dimensions and thickness was 3D printed to highlight the actuation behavior difference between rhombus patterned and solid infill samples. For our actuator arm, the primary displacement is in the xy plane with bending of the arm in the Z direction and a dynamic angular orientation. The selection of the geometrical design parameters for the actuator was done in consideration of the overall size of the samples to facilitate efficient build planning.

2.2.3. Printing

The actuator was printed using a commercially available FDM printer (ANYCUBIC i3 Mega), modified to accommodate particle-polymer composite filament printing. The extrusion temperature was set at 200 °C and the melted filament was deposited on the bed heated to 60 °C. The samples were printed with a speed of 50 mm s^{-1} with an infill density of 100%. Three different nozzles were tested, and 0.6 mm was selected to get the desired line width without clogging. The deposition directions of the infill pattern for layers were 0°. The optimized parameters for high accuracy printing were obtained by performing a statistical analysis and design of experiment (Minitab software, Version 19.2020.1) on 3D printing parameters. The best condition was determined by evaluating the results as successful and failed printing.

2.2.4. Characterization

Five sets of samples including patterned *(P samples)* and solid *(UP samples)* infills were fabricated using the above-mentioned printing process. The patterned sets of samples (P1–P4) were numbered orderly according

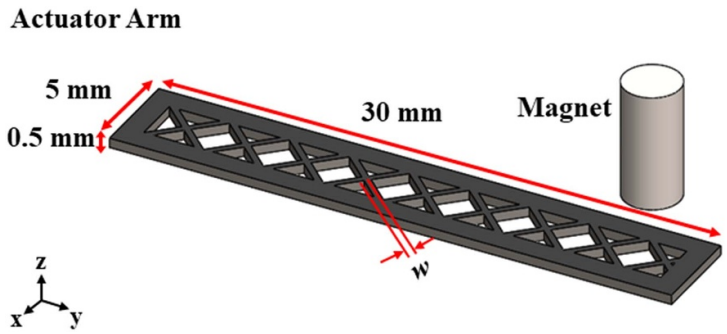

Figure 3. A digital model of the proposed actuator arm stimulated by a cylindrical NdFeB permanent magnet.

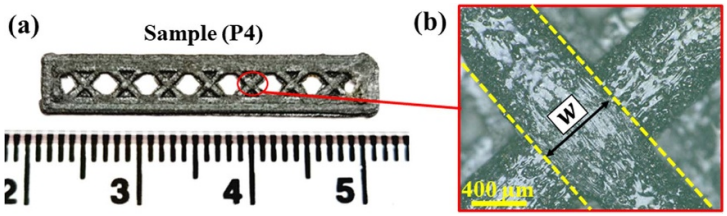

Figure 4. (a) 3D printed magnetic actuator arm illustrating sandwich rhombic lattice pattern (Sample P4 with line width of 550 μm); (b) microscopic image of the rhombic lattice interior wall's width.

to the design parameters described earlier. The wall thickness w, ranged from 400 μm to 550 μm with an interval of 50 μm. This range is adjusted to ensure the mechanical capability of the samples to serve as magnetic actuators and to provide the necessary strength and flexibility at the same time. One solid unpatterned sample (UP1) was printed to understand the behavior differences of the pattern. After fabrication of samples, experiments were designed and conducted to study the effects of different microscale pattern distribution factors on magnetic-field-responsive properties including trigger distance, bending angle and magnetic flux density of the fabricated magnetic particle-polymer actuator arms. An example of the printed sample with patterned infill is illustrated in figure 4. After evaluating the trigger distance and bending angle, the magnetic flux density at the trigger distance was measured using a precision Tesla meter TD8620. Magnetic field measurements were taken at the measured trigger distances. In addition, the mechanical properties were studied by performing tensile tests using INSTRON E3000 universal testing machine. In this test, the uniaxial tensile force was applied along the length of the sample (Y direction in figure 3). The sample was pulled with a loading rate of 1 mm s $^{-1}$ until failure of the actuator arm at room temperature.

3. Experimental results and discussion

3.1. Characterization of trigger distance

Experiments were conducted to measure the trigger distance of the actuator arm which is defined as the distance where magnetic interaction begins. To measure this distance, first, a magnet was placed above a flatly placed sample. Then it slowly approached the printed part, eventually resulting in magnetic attraction between the part and the magnet. As shown in figure 5(a), the distances where slight movements due to magnetization were observable, were recorded as experimental trigger distances. Nevertheless, it is crucial to consider that measuring the trigger distance as the minimum movement involves errors. Therefore, the results are reported based on triplicate measurements. Figure 5(b) shows trigger distance variations versus the rhombic lattice interior wall width with an average standard deviation of 0.8 mm. The trigger distance for UP1 sample was calculated to be 6.3 mm. Considering UP1 was the unpatterned solid sample, it was expected to have the lowest trigger distance. However, UP1 and P1 had almost the same triggering distance. This is because the width (400 μm) of the rhomboids made the printed sample lack the necessary concentration of ferromagnetic particles for magnetization, whereas the solid infill of the rigid sample of UP1 provided enough concentration of particles to be triggered at the same height. The trigger distance increased from 6 mm to about 8 mm as the line width changed from 400 to 550 μm. This is because the infill density and the interior pattern strongly influenced the magnetic actuation. As thicker lines contained higher amounts of ferromagnetic iron particles, the actuation started in weaker magnetic fields or in other words farther

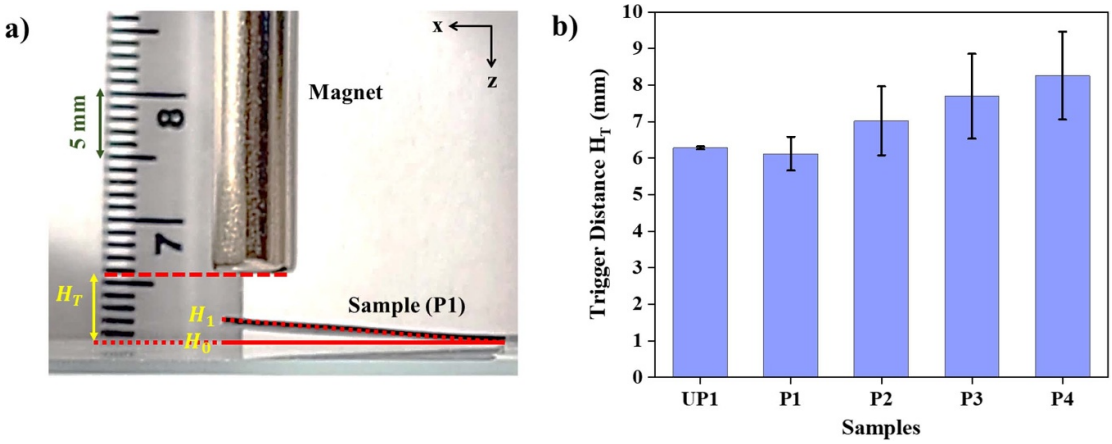

Figure 5. Characterization of trigger distance for evaluation of magnetic sensitivity of the 3D printed actuator arm. (a) Measurement method of sample P1 (H_0, H_1, and H_T represent base level, triggered level, and trigger distance, respectively); (b) trigger distances of actuator arms of P1–P4 samples printed with a layer thickness of 0.05 mm.

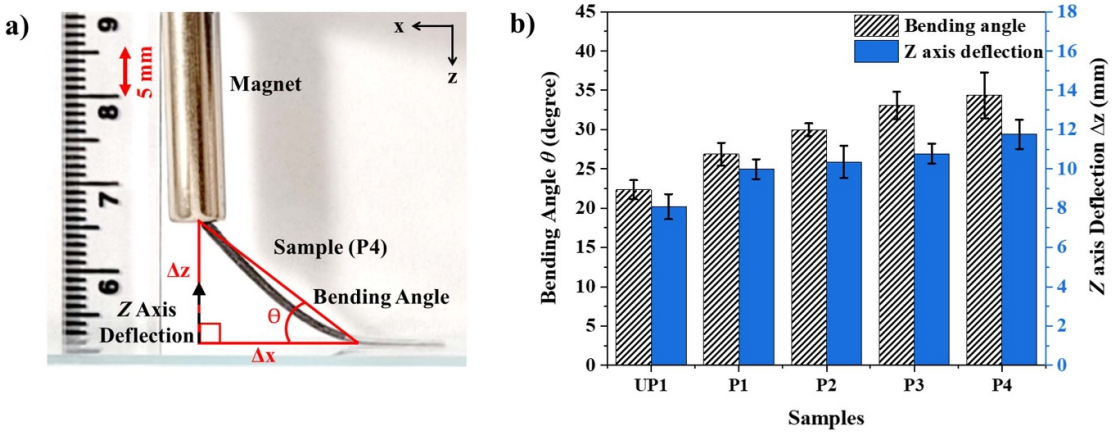

Figure 6. Evaluation Z axis deflection. (a) Illustration of the actuated state and highest deformation of the arm (sample P4); (b) experimental bending angle (θ) and Z axis deflection (Δz) of the 3D printed actuator arms printed with a layer thickness of 0.05 mm.

distances [50]. The magnetization of the structure began when the magnet was at greater distances than the other samples. The design parameters in P4 functioned the best in magnetic stimulation. This characteristic becomes vital in non-contact operations where magnetic actuation is required from a long distance [51].

3.2. Experimental tests of actuator motion (*Z* deformation)

A magnetic field strength of 6270 A m^{-1} was applied for magnetic actuation which was induced by cylindrical NdFeB permanent magnets (rare earth grade N52, from D8C, K&J Magnetics, Inc., PA, USA) with a diameter of 0.25 inch and thickness of 1 inch. The magnets were placed 5 cm above the end of an actuator arm. The actuator arm was placed on a glass slide substrate and one-third of the sample was fixed to act as the cantilever. The room temperature during the experimental tests was 298.15 K. Figure 6 shows the linear deformation of the 3D printed actuator arm under the moving magnetic field and the corresponding bending deformation. With magnetic manipulation, the actuator was able to move in the Z direction. The displacements in the Z direction and curvature of the actuator arm were measured by image analysis and calculating the bending angle using equation (1) and Z axis deflection (Δz) as illustrated in figure 6,

$$\tan^{-1}\theta = \frac{\Delta z}{\Delta x} \tag{1}$$

where θ is the bending angle, Δz is the maximum distance of the magnet attracting and bending the actuator arm, and Δx is the distance between the end of the sample and the cantilever.

Figure 6(b) illustrates the Z axis deflection and bending angle of the samples printed with a layer thickness of 0.05 mm. These values are calculated after triplicate measurements for each sample. As observed,

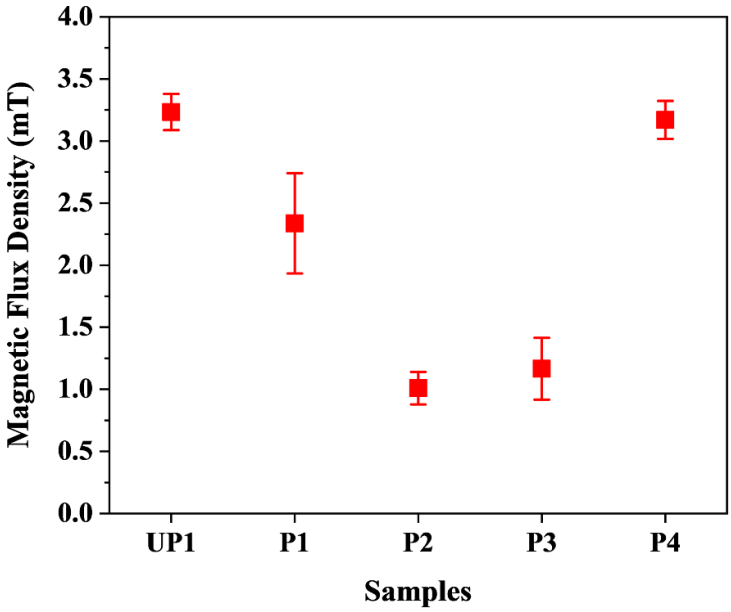

Figure 7. Magnetic flux density of samples printed with a layer thickness of 0.05 mm.

the bending angle changed from 22 to 34 degrees from UP1 (unpatterned sample) to P4 (line width of 550 μm), making this sample the most flexible actuator. The Z axis deflection values also followed similar plots. The sample with the highest bend experienced the highest deflection. The deflected position is the equilibrium point between the magnetic force imposed by the magnet and the elastic force within the composite structure [52]. This highlights the fact that the optimized design parameters ensured the desired elastic deformability even though the structure consisted of thicker lines that can limit the elasticity. However, the infill density of the rhombus pattern changed with the thicker sides. Higher infill density caused a high concentration of magnetic particles in the polymer matrix [53]. Therefore, despite the increase in magnetic sensitivity, a higher fraction of magnetic particles influenced the deformability of the sample.

3.3. Characterization of magnetic flux density

After assessing the trigger distance and the deformation characterization for magnetic responsivity, the magnetic flux density of each sample at its trigger distance was investigated to understand the magnetic properties of the 3D printed actuator arms. To ensure the repeatability of the results, the magnetic flux was measured a minimum of 3 times for each design parameter and for different samples. Figure 7 illustrates the measured magnetic flux density of the samples. As observed, the UP1 sample showed the highest magnetic flux at its trigger distance. The magnetic flux followed a descending trend as the line width increased to ~450 μm in P1 and P2, reaching 1 mT. However, the trend was changed in the P3 and P4 samples, and despite the farther trigger distances (figure 6(a)), these two samples exhibited magnetic flux densities of 1.2 and 3.2 mT respectively. This behavior can be attributed to the thicker interior lines of the rhombus structure and containing more ferromagnetic particles resulted in more magnetic flux densities. The high ferromagnetic particle concentration contributed to the more intense magnetization and magnetic flux density. It can be noted that based on the printing resolution of the printer, different layer thicknesses would cause changes in the total thickness and the mechanical behavior of the sample. As flexibility and magnetic responsivity was required, smaller layer thicknesses helped with the more flexibility and faster magnetic actuation of the sample. Even though the measured magnetic flux densities were low and weak, they still highlight the important influence of infill design dimensions on magnetic properties and consequently the actuation mechanism of magnetic arms [54, 55].

3.4. Characterization of mechanical properties

Magnetic sensitivity and high bending ability are key properties of magnetic actuators. However, high tensile strength and flexibility determine the actuators' ability and the life span for performing delicate tasks without failure [56, 57]. Figure 8 shows the effect of pattern line width on the stress-strain curves of the samples. The results are obtained by testing each design parameter three times and performing statistical analysis on the data. The elastic modulus was calculated by considering the initial linear region of the curves. The tensile properties are summarized in table 1. As observed in figure 8, unpatterned sample (UP1) exhibited linear

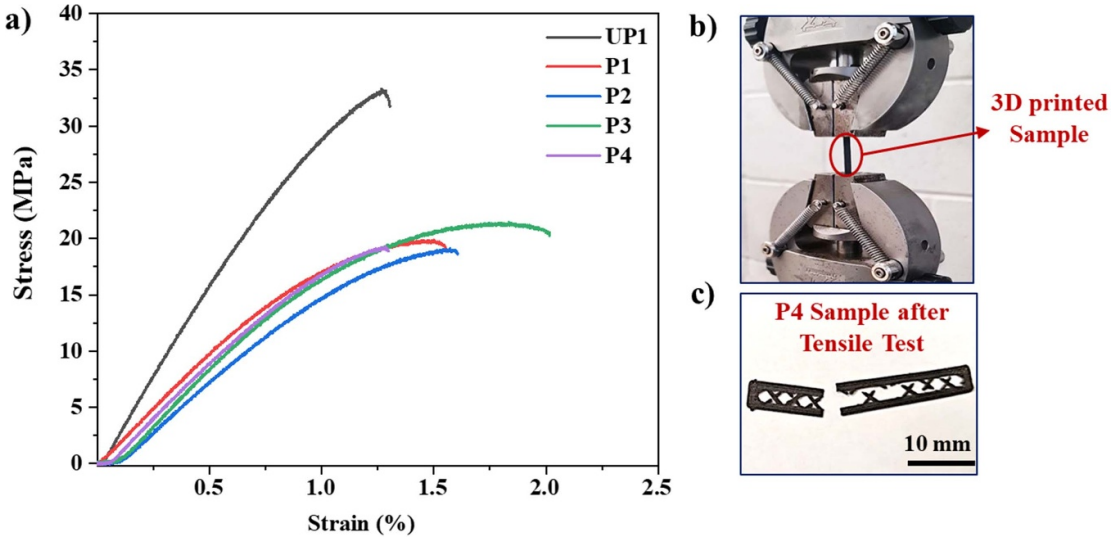

Figure 8. Tensile behavior characterization of samples printed with a layer thickness of 0.05 mm. (a) The stress versus strain curves obtained from the pull-to-failure tensile test; (b) Instron E3000 universal testing machine during the tensile test; (c) sample P4 after the pull to failure tensile test.

Table 1. The obtained values of tensile strength, Young's modulus, and elongation at break.

Sample	Tensile strength (MPa)	Young's modulus (Gpa)	Elongation (%)
UP1	35.8 ± 3.8	3.4 ± 0.3	1.4 ± 0.2
P1	19.8 ± 2.4	2.0 ± 0.3	1.7 ± 0.3
P2	17.9 ± 1.1	1.8 ± 0.1	1.6 ± 0.1
P3	20.5 ± 2.1	1.9 ± 0.3	2.1 ± 0.2
P4	17.7 ± 1.6	1.8 ± 0.1	1.3 ± 0.2

elastic behavior with high tensile strengths (35.8 MPa) and low elongation (1.4%). After the modification of the infill pattern to the rhombus pattern, the tensile behavior changed. In figure 8, P1–P4 samples exhibited low elasticity with greater ductility resulting in higher elongations. Among these samples, the *P*3 sample (figure 8) with a layer thickness of 0.05 mm showed the highest elongation at break (2.1%) and a short necking region, implying the occurrence of partial plastic deformation within the sample. This is consistent with the fact that the printing parameters including the layer thickness affect the mechanical behavior of the 3D printed samples. The *P*4 sample with the widest line width showed both relatively high tensile strength (20.5 MPa) and elongation at failure (2.1%). There was no linear relationship between the line width and the tensile strength. Also, the obtained values compared well with reported mechanical properties in literature [58, 59]. It is important to note that the iron-PLA filament is inherently more brittle than pure PLA polymer due to the presence of iron particles. In addition, the rhombus patterns within the structure can act as weak points and crack propagation sites, potentially deteriorating the properties [55, 60]. This explains the failure of the samples at edges and very close to the gripping area during the test. In general, these results highlight the fact that careful optimization of the design and 3D printing parameters is essential for obtaining desired flexibility and magnetic responsivity. Overall, the results of the tensile strength, Young's modulus and elongation show an average standard deviation of ±2.2 MPa, 0.2 GPa and 0.2%, respectively.

3.4.1. 3D printed bioinspired gripper

A magnetic gripper with two rhombus structured arms was designed and 3D printed to analyse the functionality and actuation efficiency of the gripper. The sample exhibiting the highest deformation (P4) was chosen to build a two-armed magnetic gripper named GP4. Figure 9 shows the gripping and lifting stages. As observed, the actuator arms were successfully actuated and deformed to pick up a 12.7 × 12.7 × 12.7 mm cubic object with a weight of 13.6 grams and lift without dropping (See Joyee_supplementary movie S1). To evaluate the weight-lifting capacity of the 2-armed gripper, the weights were varied from 13.6 grams to 45 grams. It was observed that GP4 actuator with P4 design parameters could grasp up to 40 grams. As mentioned earlier (figures 5 and 6), P4 had both the highest bending angle of 34 degrees and trigger distance of 8 mm, which was comparably higher than the values calculated for other samples. From this result, we can find the relationship between optimized design parameters and the necessary mechanical and magnetic

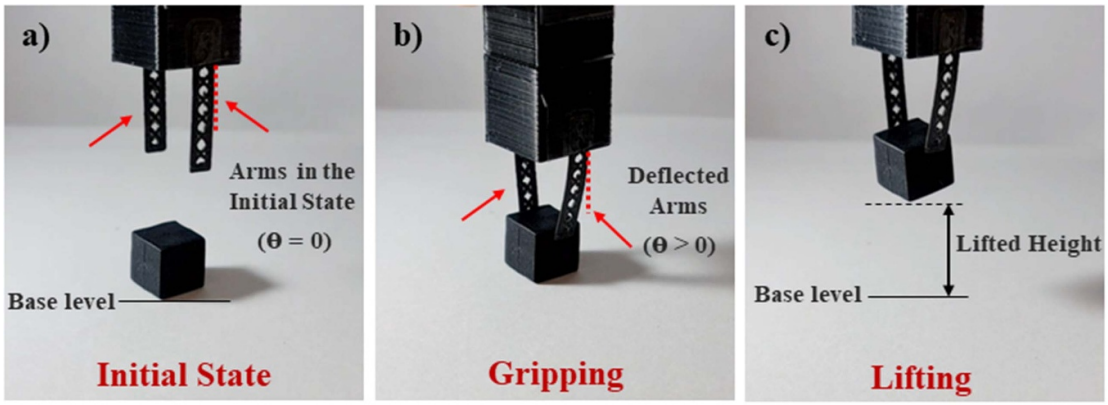

Figure 9. Different stages of bioinspired 3D printed arms gripping a 12.7 × 12.7 × 12.7 mm cubic magnet (a) 3D printed arms in initial state (before deformation); (b) actuated and deflected arms for grasping; (c) lifting the object.

properties for actuation and gripping by the actuator. Additionally, considering the versatile light-weight-high-strength properties of the 3D printed actuator arms, it can be said that the actuator arms can have potential applications in the wearable comfortable devices that can be easily embedded in co-robotics. In these devices, high flexibility, strength, and lightness are highly desirable properties [61].

4. Conclusions

This paper demonstrates a simple bioinspired design and fabrication of a magnetic stimuli-responsive gripper. Rhombic lattice sandwich structures are studied as geometric design patterns to allow maximum actuator deformation, with high-strength–low-weight structures. The design considerations also took into account the FDM printability of the magnetic particle-polymer composites. In printed parts, experiments were conducted to study the effects of different microscale pattern distribution factors on magnetic-field-responsive properties like trigger distance and magnetic flux density. It was observed that the infill density and the pattern strongly influenced magnetic actuation. Furthermore, actuator deflection and bending properties were compared for different design parameters. It was observed that an optimized line width infill pattern provided the desired deformability and mechanical behavior. In other words, a tradeoff is required in terms of weight ratio and magnetic responsiveness depending on the application. The 3D printed parts performed as actuator arms of a gripper, fulfilling the initial purpose of this work. Further future research is required to investigate more design and process parameters, for a better understanding of the relationship of actuation mechanical property with external magnetic stimuli.

The experimental investigations demonstrated in this paper will allow future research work on the 3D printing of magnetic actuators with programmed localized characteristics. This research will also be helpful in promoting the development of 3D printed biomimetic actuators with programmable integrated structures and good controllability, facilitating a wide application of potential magnetic stimulus-responsive composites in soft intelligent robots and biomedicine.

Acknowledgments

No competing financial interests exist for any author.

This research was partially funded by 'Faculty Research Grant', from the University of North Carolina at Charlotte.

Author contributions

A K designed and conducted experiments, printed parts, characterized printed parts, and prepared manuscript; E B J conceptualized the research work, supervised overall experiments, helped write and edit the manuscript.

ORCID iD

Erina Baynojir Joyee https://orcid.org/0000-0002-1506-6809

References

[1] Joyee E B and Pan Y 2020 Additive manufacturing of multi-material soft robot for on-demand drug delivery applications *J. Manuf. Process.* **56** 1178–84
[2] Joyee E B, Szmelter A, Eddington D and Pan Y 2022 3D printed biomimetic soft robot with multimodal locomotion and multifunctionality *Soft Robot.* **9** 1–13
[3] Safaee S *et al* 2022 Field-assisted additive manufacturing of polymeric composites *Addit. Manuf.* **51** 102642
[4] Li L, Scheiger J M and Levkin P A 2019 Design and applications of photoresponsive hydrogels *Adv. Mater.* **31** 1807333
[5] Chen Y, Yang J, Zhang X, Feng Y, Zeng H, Wang L and Feng W 2021 Light-driven bimorph soft actuators: design, fabrication, and properties *Mater. Horiz.* **8** 728–57
[6] Shin Y, Choi M-Y, Choi J, Na J-H and Kim S Y 2021 Design of an electro-stimulated hydrogel actuator system with fast flexible folding deformation under a low electric field *ACS Appl. Mater. Interfaces* **13** 15633–46
[7] Wang C, Sim K, Chen J, Kim H, Rao Z, Li Y, Chen W, Song J, Verduzco R and Yu C 2018 Soft ultrathin electronics innervated adaptive fully soft robots *Adv. Mater.* **30** 1706695
[8] Yin G, He Q, Zhou X, Wu Y, Li H and Yu M 2021 Printing ionic polymer metal composite actuators by fused deposition modeling technology *Int. J. Smart Nano Mater.* **12** 218–31
[9] Li Z, Huang R and Liu Z 2019 A periodic deformation mechanism of a soft actuator for crawling and grasping *Adv. Mater. Technol.* **4** 1900653
[10] Cai Z, Song Z and Guo L 2019 Thermo-and photoresponsive actuators with freestanding carbon nitride films *ACS Appl. Mater. Interfaces* **11** 12770–6
[11] Yao L, Yan H, He Y, Zhao N, Wang X, Li C, Sun L, He Y, Liu Y and Zhang J 2022 Actuation performances of catkin fibers reinforced thiol-acrylate main-chain liquid crystalline elastomer *Int. J. Smart Nano Mater.* **13** 668–90
[12] Hu W, Lum G Z, Mastrangeli M and Sitti M 2018 Small-scale soft-bodied robot with multimodal locomotion *Nature* **554** 81–85
[13] Huang H-W, Uslu F E, Katsamba P, Lauga E, Sakar M S and Nelson B J 2019 Adaptive locomotion of artificial microswimmers *Sci. Adv.* **5** eaau1532
[14] Song H, Lee H, Lee J, Choe J K, Lee S, Yi J Y, Park S, Yoo J-W, Kwon M S and Kim J 2020 Reprogrammable ferromagnetic domains for reconfigurable soft magnetic actuators *Nano Lett.* **20** 5185–92
[15] Robertson M A, Sadeghi H, Florez J M and Paik J 2017 Soft pneumatic actuator fascicles for high force and reliability *Soft Robot.* **4** 23–32
[16] Zhang Y F, Ng C J-X, Chen Z, Zhang W, Panjwani S, Kowsari K, Yang H Y and Ge Q 2019 Miniature pneumatic actuators for soft robots by high-resolution multimaterial 3D printing *Adv. Mater. Technol.* **4** 1900427
[17] Yan Y *et al* 2017 Electroactive ionic soft actuators with monolithically integrated gold nanocomposite electrodes *Adv. Mater.* **29** 1606109
[18] Tan H, Liang S, Yu X, Song X, Huang W and Zhang L 2019 Controllable kinematics of soft polymer actuators induced by interfacial patterning *J. Mater. Chem.* C **7** 5410–7
[19] Yan X *et al* 2017 Multifunctional biohybrid magnetite microrobots for imaging-guided therapy *Sci. Robot.* **2** eaaq1155
[20] Peters C, Hoop M, Pané S, Nelson B J and Hierold C 2016 Degradable magnetic composites for minimally invasive interventions: device fabrication, targeted drug delivery, and cytotoxicity tests *Adv. Mater.* **28** 533–8
[21] Jiralerspong T, Bae G, Lee J-H and Kim S-K 2020 Wireless control of two-and three-dimensional actuations of kirigami patterns composed of magnetic-particles–polymer composites *ACS Nano* **14** 17589–96
[22] Schmauch M M, Mishra S R, Evans B A, Velev O D and Tracy J B 2017 Chained iron microparticles for directionally controlled actuation of soft robots *ACS Appl. Mater. Interfaces* **9** 11895–901
[23] Tang S-Y *et al* 2018 Versatile microfluidic platforms enabled by novel magnetorheological elastomer microactuators *Adv. Funct. Mater.* **28** 1705484
[24] Ghosh A, Yoon C, Ongaro F, Scheggi S, Selaru F M, Misra S and Gracias D H 2017 Stimuli-responsive soft untethered grippers for drug delivery and robotic surgery *Front. Mech. Eng.* **3** 7
[25] Guan Z, Wang L and Bae J 2022 Advances in 4D printing of liquid crystalline elastomers: materials, techniques, and applications *Mater. Horiz.* **9** 1825–49
[26] Li Y, Li J, Li W and Du H 2014 A state-of-the-art review on magnetorheological elastomer devices *Smart Mater. Struct.* **23** 123001
[27] Chai Z, Liu M, Chen L, Peng Z and Chen S 2019 Controllable directional deformation of micro-pillars actuated by a magnetic field *Soft Matter* **15** 8879–85
[28] Shinoda H, Azukizawa S, Maeda K and Tsumori F 2019 Bio-mimic motion of 3D-printed gel structures dispersed with magnetic particles *J. Electrochem. Soc.* **166** B3235–B3239
[29] Xu T, Zhang J, Salehizadeh M, Onaizah O and Diller E 2019 Millimeter-scale flexible robots with programmable three-dimensional magnetization and motions *Sci. Robot.* **4** eaav4494
[30] Kim J, Chung S E, Choi S-E, Lee H, Kim J and Kwon S 2011 Programming magnetic anisotropy in polymeric microactuators *Nat. Mater.* **10** 747–52
[31] Roh S, Okello L B, Golbasi N, Hankwitz J P, Liu J A-C, Tracy J B and Velev O D 2019 3D-printed silicone soft architectures with programmed magneto-capillary reconfiguration *Adv. Mater. Technol.* **4** 1800528
[32] Zhu P, Yang W, Wang R, Gao S, Li B and Li Q 2018 4D printing of complex structures with a fast response time to magnetic stimulus *ACS Appl. Mater. Interfaces* **10** 36435–42
[33] Kim Y, Yuk H, Zhao R, Chester S A and Zhao X 2018 Printing ferromagnetic domains for untethered fast-transforming soft materials *Nature* **558** 274–9
[34] Qi S, Guo H, Fu J, Xie Y, Zhu M and Yu M 2020 3D printed shape-programmable magneto-active soft matter for biomimetic applications *Compos. Sci. Technol.* **188** 107973
[35] Lin C, Lv J, Li Y, Zhang F, Li J, Liu Y, Liu L and Leng J 2019 4D-printed biodegradable and remotely controllable shape memory occlusion devices *Adv. Funct. Mater.* **29** 1906569
[36] Qi S, Fu J, Xie Y, Li Y, Gan R and Yu M 2019 Versatile magnetorheological plastomer with 3D printability, switchable mechanics, shape memory, and self-healing capacity *Compos. Sci. Technol.* **183** 107817
[37] Ji Z, Yan C, Yu B, Wang X and Zhou F 2017 Multimaterials 3D printing for free assembly manufacturing of magnetic driving soft actuator *Adv. Mater. Interfaces* **4** 1700629
[38] Lantean S, Barrera G, Pirri C F, Tiberto P, Sangermano M, Roppolo I and Rizza G 2019 3D printing of magnetoresponsive polymeric materials with tunable mechanical and magnetic properties by digital light processing *Adv. Mater. Technol.* **4** 1900505

[39] Joyee E B and Pan Y 2019 A fully three-dimensional printed inchworm-inspired soft robot with magnetic actuation *Soft Robot.* **6** 333–45
[40] Zhang F *et al* 2019 *Magnetic Programming of 4D Printed Shape Memory Composite Structures* (Elsevier)
[41] Kim Y, Parada G A, Liu S and Zhao X 2019 Ferromagnetic soft continuum robots *Sci. Robot.* **4** eaax7329
[42] Zhang Y, Wang Q, Yi S, Lin Z, Wang C, Chen Z and Jiang L 2021 4D printing of magnetoactive soft materials for on-demand magnetic actuation transformation *ACS Appl. Mater. Interfaces* **13** 4174–84
[43] Ma C, Wu S, Ze Q, Kuang X, Zhang R, Qi H J and Zhao R 2020 Magnetic multimaterial printing for multimodal shape transformation with tunable properties and shiftable mechanical behaviors *ACS Appl. Mater. Interfaces* **13** 12639–48
[44] Khecho A, Ghaffari S A and Eftekhari Yekta B 2022 The influence of particle size distribution on rheological properties of fused silica pastes for direct ink writing *Int. J. Appl. Ceram. Technol.* **19** 2472–9
[45] Connors M *et al* 2019 Bioinspired design of flexible armor based on chiton scales *Nat. Commun.* **10** 5413
[46] Gao C and Li Y 2019 Mechanical model of bio-inspired composites with sutural tessellation *J. Mech. Phys. Solids* **122** 190–204
[47] Kang C, Kim S-W, Kim W, Choi D and Kim H-K 2023 Stretchable and flexible snake skin patterned electrodes for wearable electronics inspired by kirigami structure *Adv. Mater. Interfaces* **10** 2202477
[48] Alshebly Y S, Mustapha K B, Zolfagharian A, Bodaghi M, Mohamed Ali M S, Almurib H A and Nafea M 2022 Bioinspired pattern-driven single-material 4D printing for self-morphing actuators *Sustainability* **14** 10141
[49] Meyers M A, Chen P-Y, Lopez M I, Seki Y and Lin A Y M 2011 Biological materials: a materials science approach *J. Mech. Behav. Biomed. Mater.* **4** 626–57
[50] Patton M V, Ryan P, Calascione T, Fischer N, Morgenstern A, Stenger N and Nelson-Cheeseman B B 2019 Manipulating magnetic anisotropy in fused filament fabricated parts via macroscopic shape, mesoscopic infill orientation, and infill percentage *Addit. Manuf.* **27** 482–8
[51] Zhang C, Li X, Jiang L, Tang D, Xu H, Zhao P, Fu J, Zhou Q and Chen Y 2021 3D printing of functional magnetic materials: from design to applications *Adv. Funct. Mater.* **31** 2102777
[52] Li M, Wang Y, Chen A, Naidu A, Napier B S, Li W, Rodriguez C L, Crooker S A and Omenetto F G 2018 Flexible magnetic composites for light-controlled actuation and interfaces *Proc. Natl Acad. Sci.* **115** 8119–24
[53] Podstawczyk D, Nizioł M, Szymczyk P, Wiśniewski P and Guiseppi-Elie A 2020 3D printed stimuli-responsive magnetic nanoparticle embedded alginate-methylcellulose hydrogel actuators *Addit. Manuf.* **34** 101275
[54] Henderson L *et al* 2021 Altering magnetic properties of iron filament PLA using magnetic field assisted additive manufacturing (MFAAM) *APS March Meeting Abstracts J. Magn. Magn. Mater.* **538** 168320
[55] Ralchev M, Mateev V and Marinova I 2021 *Magnetic properties of FFF/FDM 3D printed magnetic material 2021 17th Conf. on Electrical Machines, Drives and Power Systems (ELMA)* (IEEE)
[56] Sachyani Keneth E, Kamyshny A, Totaro M, Beccai L and Magdassi S 2021 3D printing materials for soft robotics *Adv. Mater.* **33** 2003387
[57] Gong B *et al* 2007 Magnetic field-responsive smart polymer composites *Oligomers-Polymer Composites-Molecular Imprinting* pp 137–89
[58] Maloch J *et al* 2018 Effect of processing parameters on mechanical properties of 3D printed samples *Materials Science Forum* (Trans Tech Publications)
[59] Marşavina L, Vălean C, Mărghitaş M, Linul E, Razavi N, Berto F and Brighenti R 2022 Effect of the manufacturing parameters on the tensile and fracture properties of FDM 3D-printed PLA specimens *Eng. Fract. Mech.* **274** 108766
[60] Fafenrot S, Grimmelsmann N, Wortmann M and Ehrmann A 2017 Three-dimensional (3D) printing of polymer-metal hybrid materials by fused deposition modeling *Materials* **10** 1199
[61] Agarwal G *et al* 2016 Stretchable materials for robust soft actuators towards assistive wearable devices *Sci. Rep.* **6** 34224